E-26-611

ORO-4750-3

ASSESSMENT OF FLAT-FLUX AND FLAT-SOURCE APPROXIMATIONS IN GENERATING RESONANCE CROSS SECTIONS

by

R. A. Karam and K. D. Kirby

Final Report

Project E-26-611

R. A. Karam
Principal Investigator

School of Nuclear Engineering
Georgia Institute of Technology
Atlanta, Georgia 30332

July 1, 1975

Prepared for the U. S. Atomic Energy Commission under Contract

No. AT-(40-1)-4750

ORO-4750-3

ASSESSMENT OF FLAT-FLUX AND FLAT-SOURCE APPROXIMATIONS IN GENERATING RESONANCE CROSS SECTIONS

by

R. A. Karam and K. D. Kirby

Final Report

Project E-26-611

R. A. Karam
Principal Investigator

School of Nuclear Engineering
Georgia Institute of Technology
Atlanta, Georgia 30332

July 1, 1975

Prepared for the U. S. Atomic Energy Commission under Contract

No. AT-(40-1)-4750

ABSTRACT

Effective resonance cross sections used in the analysis of heterogeneous reactors have generally been obtained through the use of equivalence theory and/or integral transport theory. One fundamentally restrictive assumption common to equivalence theory and most integral transport methods is the flat-source approximation. The assessment of this approximation was recently completed and comprised the following:

a. Comparison of the broad group cross sections of ^{238}U in the resolved resonance region using:
   i. the flat-source approximation
   ii. the exact source distribution
   iii. the rational approximation with a Levine type factor
b. Comparisons in (a) for three types of reactors:
   i. typical ZPR-assembly
   ii. LMFBR commercial power station
   iii. light-water power reactor.

The main conclusion was that even though there were significant differences between the exactly calculated escape probabilities and those calculated with the flat-source approximation, additional differences between the general energy-dependent reciprocity and the energy-independent (but often erroneously applied as energy-dependent) reciprocity relation almost completely compensated for the error in the flat-source escape probabilities. Due to this unusual and somewhat unexpected compensating effect, the effective capture cross sections of ^{238}U in the resolved resonance region, generated by the three methods stated earlier, were essentially the same.

I. INTRODUCTION

In order to obtain effective cross sections which account for strong variations in the neutron flux in space and energy, validated methods for including the spatial component of resonance self-shielding are required. Current techniques generally include the effect of spatial self-shielding by applying an equivalence theory between homogeneous and heterogeneous cases or by integral transport theory methods which retain one of the assumptions of equivalence theory, namely, that the spatial neutron flux be flat.

There is extensive literature on the use of an equivalence principle between heterogeneous and homogeneous resonance integrals,[1-4] including extension to dense fuel lattices.[5-8] The basis of this equivalence is that the escape probability for a flat source of neutrons can be used inside and outside the fuel lump and the form of the escape probability be based on a rational approximation suggested by Wigner. The Wigner rational approximation has been noted to underestimate escape probabilities generally, and no simple correction could make the Wigner form valid over large energy ranges.[9] However, a number of correction factors have been proposed; Kelber[10,11] offered a method of determining correction factors for each resonance while preserving the equivalence relationship for each resonance. Corrections have also been made to include Dancoff-type effects for adjacent plates, and other geometry-dependent effects.[7,8,12]

The primary restriction of equivalence theory in treating heterogeneous media is that heterogeneous effects are included only through a constant, an artificial escape cross section, which appears in Wigner's rational approxi-

offered a method of determining correction factors for each resonance while preserving the equivalence relationship for each resonance. Corrections have also been made to include Dancoff-type effects for adjacent plates, and other geometry-dependent effects.[7,8,12]

The primary restriction of equivalence theory in treating heterogeneous media is that heterogeneous effects are included only through a constant, an artificial escape cross section, which appears in Wigner's rational approximation. Corrections and improvements are thus aimed at adjusting this constant if equivalence theory is to be preserved. With this approach refinements in models and computational methods are only reflected in the purely homogeneous, energy self-shielding, but spatial effects are still handled by the simpler approach.

To improve on the energy and spatial treatments Nordheim[13,14] and Chernick and Vernon[4] suggested a direct numerical integration of the integral transport equation. They noted that this approach would circumvent the necessity of picking the narrow-resonance or infinite-mass approximation and could possibly include the effects of resonance overlap and moderator absorption. Although the rational approximation for escape probabilities is not involved in this approach, most of the current integral transport methods still assume a uniform neutron source. Nordheim[14] noted that with this approach the spatial distribution of absorption is not explicitly brought out and that a closer study of spatial effects would seem to be very desirable. There are integral transport theory methods which have been developed which do not contain the flat-flux assumption, such as those of Lewis,[15,16] Kier,[17] and Olson,[18] and which in some cases could adequately treat heterogeneous effects. However, the current methods which are normally used to analyze almost all the integral data from critical facilities are

based on equivalence theory and the flat-source approximation, and for cross section averaging the more complex methods often lack the ability to give the degree of insight which the simpler methods yield.

The presence of discrepancies in comparisons between current experimental results and calculations has strengthened the desirability of the study suggested by Nordheim, because a possible source of the current discrepancy between measured and calculated reactor parameters may be due to using inappropriate methods for treating heterogeneity effects in the resonance range. The two current methods used to obtain effective resonance cross sections--equivalence theory and integral transport theory--generally contain the flat-flux approximation; hence, neither may be adequate if non-uniformity in the slowing-down sources is important. For those methods which do appear to have the capability to handle detailed heterogeneity, an improved formulation for more general application is desired. Therefore, the optimal approach would be a method to handle heterogeneous effects which could capitalize on the potentials of the integral transport theory approach but still retain some of the simplicity of formulation exhibited by equivalence theory. The development, application, and assessment of such a method have constituted the major portion of this study; in addition to eliminating the restrictions of most current methods, the generality and simple form of this method offer advantages over the few methods which include spatial effects.

II. THEORY

The fundamental definition of effective, or average, cross section is given by

$$\langle\sigma_x\rangle = \frac{\int_V \int_{\Delta E} \sigma_x(\vec{r},E)\phi(\vec{r},E)\,dE\,dV}{\int_V \int_{\Delta E} \phi(\vec{r},E)\,dE\,dV}, \tag{1}$$

where $\sigma_x(\vec{r},E)$ is the reaction cross section for the nuclide of interest which is to be averaged over an appropriate energy and volume range. $\phi(\vec{r},E)$ is the real flux and $\langle\sigma_x\rangle$ is the effective cross section of type x which, when multiplied by the flux integral, conserves the real reaction rate. For a volume which contains a uniform concentration of the nuclide, and denoting this volume as V_i, the effective cross section is written as

$$\langle\sigma_x\rangle_i = \frac{\int_{\Delta E} \sigma_x(E)\bar{\phi}_i(E)\,dE}{\int_{\Delta E} \bar{\phi}_i(E)\,dE}, \tag{2}$$

where the spatially averaged flux at energy E, $\bar{\phi}_i(E)$ has been introduced.

Knowing the energy dependence of the reaction cross section, a knowledge of the flux spectrum or an approximation to it is required to determine the effective cross section. The flux can be obtained from knowledge of the collision density contained in the slowing-down equation for heterogeneous media. The collision density may be written in accordance with the integral transport equation as given by Irving,[19]

$$\Sigma_t(\vec{r},E)\phi(\vec{r},E,\hat{\Omega}) = \int_{V'} T(\vec{r}'\rightarrow\vec{r};E,\hat{\Omega})\chi(\vec{r}',E,\hat{\Omega})\,dV' \quad , \tag{3}$$

where

$\phi(\vec{r},E,\hat{\Omega})$ = angular neutron flux at position $\vec{r}$, energy E, in the direction $\hat{\Omega}$,

$\Sigma_t(\vec{r},E)$ = total macroscopic cross section at position $\vec{r}$, energy E,

$\chi(\vec{r},E,\hat{\Omega})$ = emergent particle density, or source of neutrons emerging from position $\vec{r}$ with energy E and direction $\hat{\Omega}$,

$T(\vec{r}'\rightarrow\vec{r};E,\hat{\Omega})$ = transport kernel, or probability of a neutron at position $\vec{r}'$, energy E and direction $\hat{\Omega}$, having its next collition at position $\vec{r}$,

$$T(\vec{r}'\rightarrow\vec{r};E,\hat{\Omega}) = \Sigma_t(\vec{r},E)\, e^{-\int_{\vec{r}'}^{\vec{r}} \Sigma_t(s,E)\,ds} \frac{\delta\left(\hat{\Omega} - \frac{(\vec{r}-\vec{r}')}{|\vec{r}-\vec{r}'|}\right)}{|\vec{r}-\vec{r}'|^2} \quad . \tag{4}$$

The volume integration in Eq. 3 is over all space, and the delta function is in the transport kernel in order to include only those sources which, when headed in the direction $\hat{\Omega}$ from $\vec{r}'$, can reach position $\vec{r}$.

The neutron source distribution, $\chi(\vec{r},E,\hat{\Omega})$ consists of all sources of neutrons due to elastic scattering, inelastic scattering, fission, external sources, or any other applicable mechanism. Writing only the elastic scattering portion explicitly, the neutron source distribution density may be expressed as

$$\chi(\vec{r},E,\hat{\Omega}) = \int_{E'}\int_{\hat{\Omega}'} \Sigma_s(\vec{r};E'\hat{\Omega}'\rightarrow E,\hat{\Omega})\phi(\vec{r},E',\hat{\Omega}')\,d\hat{\Omega}'\,dE' + Q(\vec{r},E,\hat{\Omega}) \quad , \tag{5}$$

where

$\Sigma_s(\vec{r};E',\hat{\Omega}'\rightarrow E,\hat{\Omega})$ = differential elastic scattering cross section at $\vec{r}$, for an incident neutron of energy E' and direction $\hat{\Omega}'$, emerging from the collision with energy E and direction $\hat{\Omega}$,

$Q(\vec{r},E,\hat{\Omega})$ = source of neutrons, other than elastic scattering, emerging from position $\vec{r}$ with energy E and direction $\hat{\Omega}$.

To perform the cross section averaging noted in Eq. 1, the total flux $\phi(\vec{r},E)$ is desired rather than the angular flux. To obtain this Eq. 3 is integrated over all directions; the volume integration can also be expressed as a sum of integrals over individual volumes V_j which make up the system to give

$$\Sigma_t(\vec{r},E)\phi(\vec{r},E) = \sum_j \int_{V_j}\int_{\hat{\Omega}} T(\vec{r}'\rightarrow\vec{r};E,\hat{\Omega})\chi(\vec{r}',E,\hat{\Omega})\,d\hat{\Omega}dV' \quad . \tag{6}$$

One can then define

$$P_j(\vec{r},E) = \frac{\int_{V_j}\int_{\hat{\Omega}} T(\vec{r}'\rightarrow\vec{r};E,\hat{\Omega})\chi(\vec{r}',E,\hat{\Omega})\,d\hat{\Omega}dV'}{\int_{V_j}\int_{\hat{\Omega}} \chi(\vec{r}',E,\hat{\Omega})\,d\hat{\Omega}dV'} \tag{7}$$

which is the number of neutrons from sources in V_j which have their next collision at position $\vec{r}$, divided by the total source in V_j. This is merely the average probability that a neutron from sources in V_j will have its next collision at $\vec{r}$. With the use of Eq. 7 one may rewrite Eq. 6 as

$$\Sigma_t(\vec{r},E)\phi(\vec{r},E) = \sum_j P_j(\vec{r},E) \int_{V_j}\int_{\hat{\Omega}} \chi(\vec{r}',E,\hat{\Omega})\, d\hat{\Omega}\, dV' \quad . \tag{8}$$

For the case in which the volume of interest for cross section averaging is V_i, the total collision rate in the volume is obtained by integrating Eq. 8 over V_i. With the integration, the factor $\int_{V_i} P_j(\vec{r},E)$ is introduced and, based on the interpretation of $P_j(r,E)$, it can be described as the average probability that a neutron from sources in V_j will make its next collision in V_i. This is simply the escape probability from V_j to V_i which may be written as

$$\int_{V_i} P_j(\vec{r},E)\, dV = P_{j\to i}(E) \quad . \tag{9}$$

Since $P_i(\vec{r},E)$ is the probability that neutrons from V_i will collide at point $\vec{r}$, then the integral over all space will be unity provided that leakage from the reactor system is considered. Utilizing this property, the collision rate in V_i can now be written as

$$\Sigma_{t_i}(E)\bar{\phi}_i(E)V_i = \left(1 - \sum_j P_{i\to j}(E)\right) \bar{\chi}_i(E)V_i + \sum_j P_{j\to i}(E)\bar{\chi}_j(E)V_j \quad , \tag{10}$$

where the summation is over all volumes other than V_i, spatially averaged quantities have been introduced, and one of the $P_{i\to j}(E)$ is the probability of a neutron in V_i completely escaping the reactor.

The collision rate expression developed above is a general basis for developing effective cross sections for heterogeneous media. The expression is completely general with only the restriction that cross sections are space independent within each volume V_j. The same expression

may be obtained by a simple neutron balance, but the above approach gives the required formulation of the escape probabilities in order that Eq. 10 be exact. Most current methods of obtaining effective cross sections for heterogeneous media also begin with this collision rate expression, but various restrictions on spatial effects are immediately imposed.

Reciprocity Relations

In order to solve the collision rate expression given by Eq. 10 the sources and escape probabilities must be determined. However, before attempting to obtain each escape probability, additional development using the reciprocity properties of the transport equation can allow escape probabilities to be related to each other.

The general, energy-dependent reciprocity property of the transport equation as noted by Bell[1] is

$$\int_V\int_E\int_{\hat{\Omega}} S(\vec{r},E,\hat{\Omega})\phi^*(\vec{r},E,\hat{\Omega})\,d\hat{\Omega}dEdV = \int_V\int_E\int_{\hat{\Omega}} S^*(\vec{r},E,\hat{\Omega})\phi(\vec{r},E,\hat{\Omega})\,d\hat{\Omega}dEdV \quad , \tag{11}$$

where ϕ and ϕ^* are the real and adjoint flux solutions of the real and adjoint energy-dependent transport equations with arbitrary external sources,

$$L\phi = -S \quad \text{and} \quad L^*\phi^* = -S^*. \tag{12}$$

L and L* are the transport operator and adjoint operator, respectively, and S and S* are real and adjoint sources. This relation can be used to determine relationships between escape probabilities by defining the arbitrary sources as

$$\begin{aligned} S &= \chi(\vec{r},E,\hat{\Omega})\,\delta(E-E_o) \quad , \quad \text{for r in } V_i, \\ &= 0 \qquad\qquad\qquad\quad , \quad \text{otherwise;} \end{aligned} \tag{13}$$

$$S^* = \Sigma_d(\vec{r},E,\hat{\Omega})\,\delta(E-E_o) \quad , \text{ for r in } V_j, \qquad (14)$$
$$= 0 \quad , \text{ otherwise.}$$

E_o is some arbitrary energy of interest and δ is the Dirac delta function. The general interpretation of $\Sigma_d(\vec{r},E,\hat{\Omega})$ is an arbitrary detector response function; in this case the response of interest is a collision in V_j, so $\Sigma_d(\vec{r},E,\hat{\Omega}) = \Sigma_{t_j}(E)$. With these sources, Eq. 11 then becomes

$$\int_{V_i}\int_{\hat{\Omega}} \chi(\vec{r},E_o,\hat{\Omega})\phi^*(\vec{r},E_o,\hat{\Omega})\,d\hat{\Omega}dV = \int_{V_j}\int_{\hat{\Omega}}\Sigma_{t_j}(E_o)\phi(\vec{r},E_o,\hat{\Omega})\,d\hat{\Omega}dV \; . \qquad (15)$$

Equation 15 is now divided by $\int_{V_i}\int_{\hat{\Omega}}\chi(\vec{r},E_o,\hat{\Omega})\,d\hat{\Omega}dV$ which yields

$$\frac{\int_{V_i}\int_{\hat{\Omega}}\chi(\vec{r},E_o,\hat{\Omega})\phi^*(\vec{r},E_o,\hat{\Omega})\,d\hat{\Omega}dV}{\int_{V_i}\int_{\hat{\Omega}}\chi(\vec{r},E_o,\hat{\Omega})\,d\hat{\Omega}dV} = \frac{\int_{V_j}\int_{\hat{\Omega}}\Sigma_{t_j}(E_o)\phi(\vec{r},E_o,\hat{\Omega})\,d\hat{\Omega}dV}{\int_{V_i}\int_{\hat{\Omega}}\chi(\vec{r},E_o,\hat{\Omega})\,d\hat{\Omega}dV} \; . \qquad (16)$$

Inspection of the right-hand side of Eq. 16 shows that it is the collision rate at energy E_o in volume V_j due to a source χ only in volume V_i, divided by that total source strength. This is the same as the escape probability from V_i to V_j at energy E_o. On the left-hand side of the above equation one can also note that the ratio of the integrals could be interpreted as an average adjoint flux with the source χ as the weighting function. Thus with

$$P_{i\to j}(E_o) = \frac{\int_{V_j}\int_{\hat{\Omega}}\Sigma_{t_j}(E_o)\phi(\vec{r},E_o,\hat{\Omega})\,d\hat{\Omega}dV}{\int_{V_i}\int_{\hat{\Omega}}\chi(\vec{r},E_o,\hat{\Omega})\,d\hat{\Omega}dV} \; , \qquad (17)$$

and defining

$$\hat{\phi}_i^*(E_o) = \frac{\int_{V_i}\int_{\hat{\Omega}} \chi(\vec{r},E_o,\hat{\Omega})\phi^*(\vec{r},E_o,\hat{\Omega})\,d\hat{\Omega}dV}{\int_{V_i}\int_{\hat{\Omega}} \chi(\vec{r},E_o,\hat{\Omega})\,d\hat{\Omega}dV}\ , \tag{18}$$

one can write Eq. 16 as

$$\hat{\phi}_i^*(E_o) = P_{i\to j}(E_o)\ . \tag{19}$$

Thus the escape probability is obtained for an arbitrary source shape in one volume in terms of a weighted average of the adjoint flux solution due to a uniform source in another volume. Since the only restriction on the volumes is that the cross section of each be space independent, a volume may have arbitrary shape, even be subdivided, and the above expression still holds.

The same development which led to Eq. 19 can be applied reversing the roles of V_i and V_j, or the indices may be reversed in Eq. 19 since it is general to yield

$$\hat{\phi}_j^*(E_o) = P_{j\to i}(E_o)\ . \tag{20}$$

The ratio of Eq. 20 to Eq. 19 then yields a generalized reciprocity relation,

$$\frac{P_{j\to i}(E_o)}{P_{i\to j}(E_o)} = \frac{\hat{\phi}_j^*(E_o)}{\hat{\phi}_i^*(E_o)}\ . \tag{21}$$

In comparison to the generalized reciprocity relation of Eq. 21, it is useful to examine the generally used reciprocity relation. For an

isotropic neutron source, distributed uniformly in space, the reciprocity properties of the transport equation yield the following relationship between escape probabilities,[1]

$$P_{j\to i}^{flat}(E_o)V_j\Sigma_{t_j}(E_o) = P_{i\to j}^{flat}(E_o)V_i\Sigma_{t_i}(E_o) \ . \tag{22}$$

Comparing the generalized reciprocity relation of Eq. 21 with the flat-flux reciprocity relation of Eq. 22, one can readily introduce a parameter

$$f_{ij}(E) = \frac{\hat{\phi}_j^*(E)V_j\Sigma_{t_j}(E)}{\hat{\phi}_i^*(E)V_i\Sigma_{t_i}(E)} \ , \tag{23}$$

which can be used to rewrite the generalized reciprocity relation as

$$\frac{P_{j\to i}(E)V_j\Sigma_{t_j}(E)}{P_{i\to j}(E)V_i\Sigma_{t_i}(E)} = f_{ij}(E) \ . \tag{24}$$

In this form the new parameter can be interpreted as a nonuniformity parameter which is unity when the neutron source is flat. Introducing this parameter into the collision rate expression (Eq. 10), the result is

$$\Sigma_{t_i}(E)\overline{\phi}_i(E) = \left(1 - \sum_j P_{i\to j}(E)\right)\overline{\chi}_i(E) + \sum_j f_{ij}(E)P_{i\to j}(E)\frac{\Sigma_{t_i}(E)}{\Sigma_{t_j}(E)}\overline{\chi}_j(E). \tag{25}$$

This expression may then be used for arbitrary nonuniform sources, and for uniform sources it correctly reduces to the flat-flux approximation.

Escape Cross Section

The collision rate expression of Eq. 25 can be simplified by expressing the escape probability in a form similar to that introduced by Wigner in his work on lumped absorbers.[20] Wigner proposed a "rational approximation" for the escape probability for a flat source of neutrons which approaches the correct value for the extremes of a large or small volume. The rational approximation is given by

$$P_{esc} = \frac{\Sigma_e}{\Sigma_t(E) + \Sigma_e} . \tag{26}$$

where Σ_e is an artificial escape cross section, a constant with the units of macroscopic cross section, defined by

$$\Sigma_e = \frac{A}{4V}, \tag{27}$$

A is the surface area and V is the volume of the region.

The validity of Wigner's rational approximation has been questioned several times noting that it generally underpredicts the exact escape probability for a uniform source.[1,3,9,10] However, the simplicity of it has been so advantageous that it is widely used. The primary restriction that causes limitation is that the escape cross section, even with corrections, be a constant. However, by defining an energy-dependent escape cross section as that which preserves the correct escape probability, the simplicity of the form of Wigner's rational approximation can be introduced into the generalized development.

Similar to Eq. 26, introduce an energy dependent escape cross section $\Sigma_e^{ij}(E)$ such that the escape probability from V_i to V_j is given by

$$P_{i\to j}(E) = \frac{\Sigma_e^{ij}(E)}{\Sigma_{t_i}(E) + \Sigma_e^{ij}(E)} \cdot \tag{28}$$

The escape cross section is thus defined as

$$\Sigma_e^{ij}(E) = \frac{\Sigma_{t_i}(E) P_{i\to j}(E)}{1 - P_{i\to j}(E)} \cdot \tag{29}$$

The escape probability as given by Eq. 28 can now be substituted into the collision rate expression shown in Eq. 25. For the case of a two-region problem, with either one region isolated within another one or a repeating arrangement of two volumes, Eq. 25 reduces to

$$\Sigma_{t_i}(E)\bar{\phi}_i(E) = \frac{\Sigma_{t_i}(E)}{(\Sigma_{t_i}(E) + \Sigma_e^{ij}(E))} \bar{\chi}_i(E) + f_{ij}(E) \frac{\Sigma_e^{ij}(E)}{(\Sigma_{t_i}(E) + \Sigma_e^{ij}(E))} \frac{\Sigma_{t_i}(E)}{\Sigma_{t_j}(E)} \bar{\chi}_j(E) \cdot \tag{30}$$

From this equation one can readily solve for the spatial average of the flux as

$$\bar{\phi}_i(E) = \frac{\bar{\chi}_i(E) + f_{ij}(E) \frac{\Sigma_e^{ij}(E)}{\Sigma_{t_j}(E)} \bar{\chi}_j(E)}{\Sigma_{t_i}(E) + \Sigma_e^{ij}(E)} \cdot \tag{31}$$

One has thus obtained a generalized expression for the flux which is simple in form but which can include detailed spatial effects as well as spectral effects.

To demonstrate the generality of this approach it may be easily

shown that it correctly reduces to equivalence theory under the usual assumptions. The basic assumptions of equivalence theory and their implications in this approach are:

1. Narrow resonance approximation -- $\bar{\chi}(E) = \Sigma_s/E$,
2. Flat-flux approximation -- $f_{ij}(E) = 1$,
3. Wigner's rational approximation -- Σ_e = constant.

Also imposing constant scattering cross section and no absorption in the moderator region, Eq. 31 becomes

$$\bar{\phi}_i(E) = \frac{(\Sigma_{s_i} + \Sigma_e)}{(\Sigma_{t_i}(E) + \Sigma_e)} \frac{1}{E} , \qquad (32)$$

which yields the usual equivalence properties.[1,4] Here Σ_e appears as merely an addition to the scattering cross section, so the heterogeneous case can be made equivalent to a homogeneous case by merely augmenting the scattering cross section by Σ_e. It should be noted, however, that only after imposing the above assumptions does the general method reduce to equivalence theory.

To determine cross section averages, the general flux expression of Eq. 31 can be substituted into the averaging expression given by Eq. 2; one thus has the basis of a generalized method of generating effective resonance cross sections with freedom from restrictive assumptions. The simple form and general nature of this method should allow easy assessment of the influence of any of the parameters, and this property yields distinct contributions. Since each parameter has an analog in current methods, sophisticated analysis could be used to determine parameters of the flux expression, thus allowing evaluation of the magnitude and sources of restrictions in

current methods. Also, with the same general method of cross section averaging one could easily and correctly include standard approximations by merely adjusting the appropriate parameter in the general expression.

III. COMPUTATIONAL APPROACH

In order to investigate the general method of cross section averaging described above, computations were performed to examine the fundamental parameters and the effects of spatial nonuniformity on effective cross sections. Determination of the fluxes and sources is required to subsequently obtain escape probabilities and the nonuniformity parameters $f(E)$ and $\Sigma_e(E)$. Consequently, a method of determining the flux and source distributions was developed which would also yield the nonuniformity parameters. Solution of the integral transport equation for the real neutron flux and source is the basis of the method; the nonuniformity parameters can be determined by appropriate solution for the real flux only, so solution for both the real and adjoint flux is not used here.

For the purposes of this work the computational development was limited to the study of heterogeneous effects in a one-dimensional slab model of a two-region cell. This should be adequate for the determination of the nonuniformity factors and assessment of the general method. The computational procedure can be outlined with the following steps. The neutron flux and source solutions to the integral transport equations as expressed by Eqs. 3 and 5 are first obtained for an infinitely repeating lattice of two-region cells. After obtaining the source distribution, the components of the flux distribution due to the source in one region, then the other, are obtained. This approach allows determination of the escape probabilities as given by Eq. 17. From the escape probabilities the nonuniformity factors $f(E)$ and $\Sigma_e(E)$ can then be obtained by Eqs. 24

and 29, respectively.

For an infinite, repetitive lattice in slab geometry, the integral transport equation can be written as

$$\phi(x,E) = \int_{x'=-\infty}^{\infty} \int_{R=|x-x'|}^{\infty} \frac{e^{-\frac{R}{|x-x'|}\int_{x'}^{x} \Sigma_t(S,E)\,dS}}{2R} \chi(x',E)\,dR\,dx' \qquad (33)$$

where x and x′ are spatial positions and R is the chord length for integration. For the source, the scattering and external components were assumed to be isotropic, resulting in

$$\chi(x,E) = \int_{E'} \Sigma_S(x,E'\rightarrow E)\phi(x,E')\,dE' + Q(x,E) \ . \qquad (34)$$

Taking advantage of symmetry and periodic conditions within the lattice, the infinite integral of Eq. 33 can be changed to an integration over half the unit cell. The resulting integral equation can be expressed as

$$\phi(x,E) = \int_{o}^{b} \frac{\chi(x',E)}{2} T(x,x',E)\,dx', \qquad (35)$$

where b is half the cell thickness for two adjacent slabs with the origin in the center of one slab, and

$$T(x,x',E) = \sum_{m=-\infty}^{\infty} \{E_1[\tau(x,x'+m2b,E)] + E_1[\tau(x,-x'+m2b,E)]\} \ . \qquad (36)$$

The above expression defines the transport kernel for an infinite lattice in slab geometry where E_1 is the first order exponential integral and τ is the optical thickness,

$$\tau(x,x',E) = \int_{x'}^{x} \Sigma_t(s,E)ds. \tag{37}$$

Provided one knows the source distribution in the above expression the integration could be carried out to obtain the flux distribution. The two distributions are interdependent, however, and the solutions must be obtained simultaneously. Assuming the presence of several isotopes and indicating each with an index i, the elastic scattering source can be more adequately formulated and Eq. 34 becomes

$$\chi(x,E) = \sum_i \int_E^{E/\alpha_i} \frac{\Sigma_{Si}(x,E')}{(1-\alpha_i)E'} \phi(x,E')dE' + Q(x,E) \ . \tag{38}$$

$\Sigma_S(x,E')$ is the total elastic scattering cross section at energy E' and

$$\alpha = \left(\frac{A-1}{A+1}\right)^2 \ , \tag{39}$$

where A is the atomic weight of a particular isotope.

To solve Eqs. 35 and 38 together a discrete mesh of spatial and energy points is imposed. These meshes are simply $x = x_n$, for n = 1, . . ., N, and $E = E_g$, for g = 1, . . ., G, where $x_1 = 0$, $x_N = b$, and one of the points $x_K = a$, the interface position between the two regions; for the energy mesh, E_1 is the highest energy of interest and the remaining values decrease in energy. Between the energy mesh points the scattering rate for each isotope is assumed to be a linear function of energy, that is,

$$\Sigma_{Si}(x,E)\phi(x,E) = \tag{40}$$

$$\frac{(E-E_g)\Sigma_{Si}(x,E_{g-1})\phi(x,E_{g-1}) + (E_{g-1}-E)\Sigma_{Si}(x,E_g)\phi(x,E_g)}{E_{g-1} - E_g} .$$

Above the energy E_1, the asymptotic flux spectrum is assumed,

$$\Sigma_{Si}(x,E)\phi(x,E) = \Sigma_{Si}(x,E_1)\phi(x,E_1)\frac{E_1}{E} , \qquad E \geq E_1 . \tag{41}$$

Between the spatial mesh points the source distribution is assumed to be a linear function of position,

$$\chi(x,E) = \frac{(x-x_n)\chi(x_{n+1},E) + (x_{n+1}-x)\chi(x_n,E)}{x_{n+1} - x_n} , \tag{42}$$

so the integral transport problem becomes the determination of the flux and source at the space-energy nodes -- x_n, E_g. The energy mesh approach noted above is modeled after the treatment used in the GAROL code[21] and the spatial mesh treatment reflects that used in the RABID code.[18] The use of them together here is felt to capitalize on the most advantageous aspects of both codes.

By imposing the energy mesh the integration required for the source determination can be carried out, and by inserting the spatial shape of the slowing down source the integration of Eq. 35 can also be expressed in a manner which is readily solvable by an iterative technique. The steps outlined above were implemented into a computer code to determine the detailed effects of heterogeneity due to an isolated resonance for a material in region 1 of the two-region, slab cell configuration. Integrations in-

volving the transport kernel result in a series of higher order exponential integrals and evaluation of the kernels is performed similar to that used in the RABID code.[18] The highest energy point is required to be at least E_o/α^3, where E_o is the resonance energy and α is for the resonance isotope. Thirty mesh points each are allowed for energy and space with arbitrary spacing. To obtain a reasonable mesh, energy spacing is determined by inspection after generating the resonance cross sections. The spatial mesh selection is quite important due to the spatial averaging that is to be performed. To assure that spatial points are selected which will yield acceptable resolution for all energies, an approximate solution is examined. A boundary condition at the highest energy is required, and the iteration process can step down in energy from there to determine the final solution. To eliminate the possible accumulation of any small errors a kernel normalization and a neutron conservation relation similar to those noted by Lewis[15] are used.

With the determination of the final flux and source solutions, the escape probabilities and nonuniformity factors can then be obtained. The escape probabilities can be determined by obtaining the flux solution in one region due to the source in the other region. This can be stated by

$$P_{1\to 2}(E) = \frac{\int_{V_2} \Sigma_{t_2}(E)\phi^1(x,E)\,dx}{\int_{V_1} \chi(x,E)\,dx}, \tag{43}$$

or

$$P_{1\to 2}(E_g) = \frac{\Sigma_t^{2g}\,\bar{\phi}^1_{2g}\,T_2}{\bar{\chi}_{1g}\,T_1}, \tag{44}$$

where $\bar{\phi}^1_{2g}$ is the average flux in region 2 due only to sources in region 1. The escape probability from region 2 to region 1 can be determined similarly by obtaining $\bar{\phi}^2_{1g}$, the average flux in region 1 due only to sources in region 2, to yield

$$P_{2\to1}(E_g) = \frac{\Sigma_t^{1g}\ \bar{\phi}^2_{1g}\ T_1}{\bar{\chi}_{2g}\ T_2} \ . \tag{45}$$

The escape cross section can then be expressed by

$$\Sigma_e(E_g) = \frac{\Sigma_t^{1g}\ P_{1\to2}(E_g)}{1-P_{1\to2}(E_g)} \ , \tag{46}$$

or by dividing by the atom density of the resonance absorber, N_r, an escape cross section per atom of absorber can be defined by

$$\sigma_e(E_g) = \Sigma_e(E_g)/N_r \ . \tag{47}$$

Finally, the expression for the nonuniformity factor f(E) can be obtained by using Eqs. 31 and 32 to reduce the general relation of Eq. 24 from the form

$$f(E_g) = \frac{P_{2\to1}(E_g)\ \Sigma_t^{2g}\ T_2}{P_{1\to2}(E_g)\ \Sigma_t^{1g}\ T_1} \tag{48}$$

to

$$f(E_g) = \frac{\bar{\phi}^2_{1g}\ \bar{\chi}_{1g}\ T_1}{\bar{\phi}^1_{2g}\ \bar{\chi}_{2g}\ T_2} \ . \tag{49}$$

Since only one isolated resonance is examined in the computation,

the cross sections for the non-resonance materials are assumed to be constant. Any degree of absorption is allowed for these materials though. The resonance cross sections include s-wave scattering only and are determined from routines for evaluating the Doppler broadened shape functions from the ERIC-2 code[22] and the RABBLE code.[23]

To perform cross section averaging, the nonuniformity effects must be expressed for a wide energy range including many resonances. For this study a parametric variation of resonance parameters was used to generate data from which the nonuniformity factors for resonances of ^{238}U were obtained by interpolation. The resulting data allow the description of nonuniformity effects due to isolated resonances on the flux through

$$\bar{\phi}_1(E) = \frac{\bar{\chi}_1(E) + f(E)\,\frac{\Sigma_e(E)}{\Sigma_{t2}(E)}\,\bar{\chi}_2(E)}{\Sigma_{t1}(E) + \Sigma_e(E)} \,. \tag{50}$$

To perform the cross section averaging the energy integration is performed resonance by resonance using a Romberg numerical quadrature.[24] The exact flat treatment and equivalence theory are also examined and treated as special cases of the general method. For the exact flat treatment f(E) is set equal to unity and the escape cross section is determined from

$$\Sigma_e^{flat}(E) = \frac{\Sigma_{t1}(E)\; P_{1\to2}^{flat}(E)}{1 - P_{1\to2}^{flat}(E)} \,. \tag{51}$$

For this case the escape probability for a flat source can be written[14]

$$P_{1\to2}^{flat}(E) = \frac{P_{esc}(E)\,(1-C)}{1 - (1-2\Sigma_{t1}(E)T_1P_{esc}(E))C} \,, \tag{52}$$

with

$$P_{esc}(E) = \frac{1}{\Sigma_{t1}(E)T_1}\left[0.5 - E_3(\Sigma_{t1}(E)T_1)\right] , \tag{53}$$

and the Dancoff correction is given by[25]

$$C = 2E_3(\Sigma_{t2}T_2) . \tag{54}$$

For equivalence theory f(E) is also unity and Σ_e is constant. The value of Σ_e is determined by the procedure given by Travelli[12] for a slab lattice, where

$$\Sigma_e = \frac{1.09}{2T_1}(1-C) , \tag{55}$$

with

$$1-C = \gamma_B + 1.7\gamma_B^4(1-\gamma_B) , \tag{56}$$

and

$$\gamma_B = \left(1 + \frac{1}{2\Sigma_{t2}T_2}\right)^{-1} . \tag{57}$$

In each of the above cases the narrow resonance approximation is used for all materials. Within the same general method then there are three different degrees of treating heterogeneity, and with these three treatments available together, comparisons can be made on a consistent basis and the relative effects of heterogeneity by the different treatments readily assessed.

IV. RESULTS

Using the methods outlined above, calculations were performed to assess the characteristics of the general method and the effect of nonuniformity on effective resonance cross sections. The behavior of the nonuniformity parameter $f(E)$ and escape cross section $\sigma_e(E)$ are determined for resonances of ^{238}U for a two-region cell of ZPR-6 Assembly 5[26] using the integral transport theory method of Section III. The same method is then used for a parametric assessment of the nonuniformity parameters for the resolved resonance range of ^{238}U to characterize the parameters required for cross section averaging. Effective cross sections are then obtained using the general method, and comparisons are made between the nonuniform treatment and more approximate treatments.

Integral Transport Theory Analysis

The effect of spatial nonuniformity in the slowing-down source was examined for an equivalent two-region cell for the core region of ZPR-6 Assembly 5. A complete description of the plate loading pattern for Assembly 5 is given in Reference 26. There are several ^{238}U plates distributed throughout the actual cell, twelve 1/8 inch plates and two 1/16 inch plates; the two-region cell is a single 1/8 inch plate with the associated outer region representing a proportional homogenization of the other types of plates. The resulting cell description is given in Table I. The nonuniformity parameter $f(E)$ and the escape cross section around three different ^{238}U resonances were examined. The three resonances represent

a large, moderate, and weak resonance; the resonance parameters of these resonances are given in Table II.

Table I. Composition for Two-Region Cell of ZPR-6 Assembly 5

	Nuclide	Concentration (10^{24} cm^{-3})
^{238}U Plate (0.3175 cm)	^{238}U	0.04783
Outer Region (1.0264 cm)	^{235}U	0.00202
	C	0.01693
	Na	0.01205
	Fe	0.01184
	Ni	0.00148
	Cr	0.00313

Table II. Selected ^{238}U Resonance Parameters

Peak Energy(eV)	Neutron Width(eV)	Capture Width(eV)	Total Width(eV)
189.6	0.1690	0.0247	0.1937
518.3	0.0555	0.0244	0.0799
1098.1	0.0170	0.0235	0.0405

The energy- and spatial-dependent fluxes and sources were determined for each of the three resonances of ^{238}U; the energy-dependent fluxes at the center of the plate, at the plate/outer region interface, and at the center of the outer region, or edge of the cell, for the 189.6 eV resonance are shown in Fig. 1. In each case the flux is normalized to unity, and uniform across the cell, at E_o/α^3 or $E_o + 50\,\Gamma_t$, whichever is larger. The

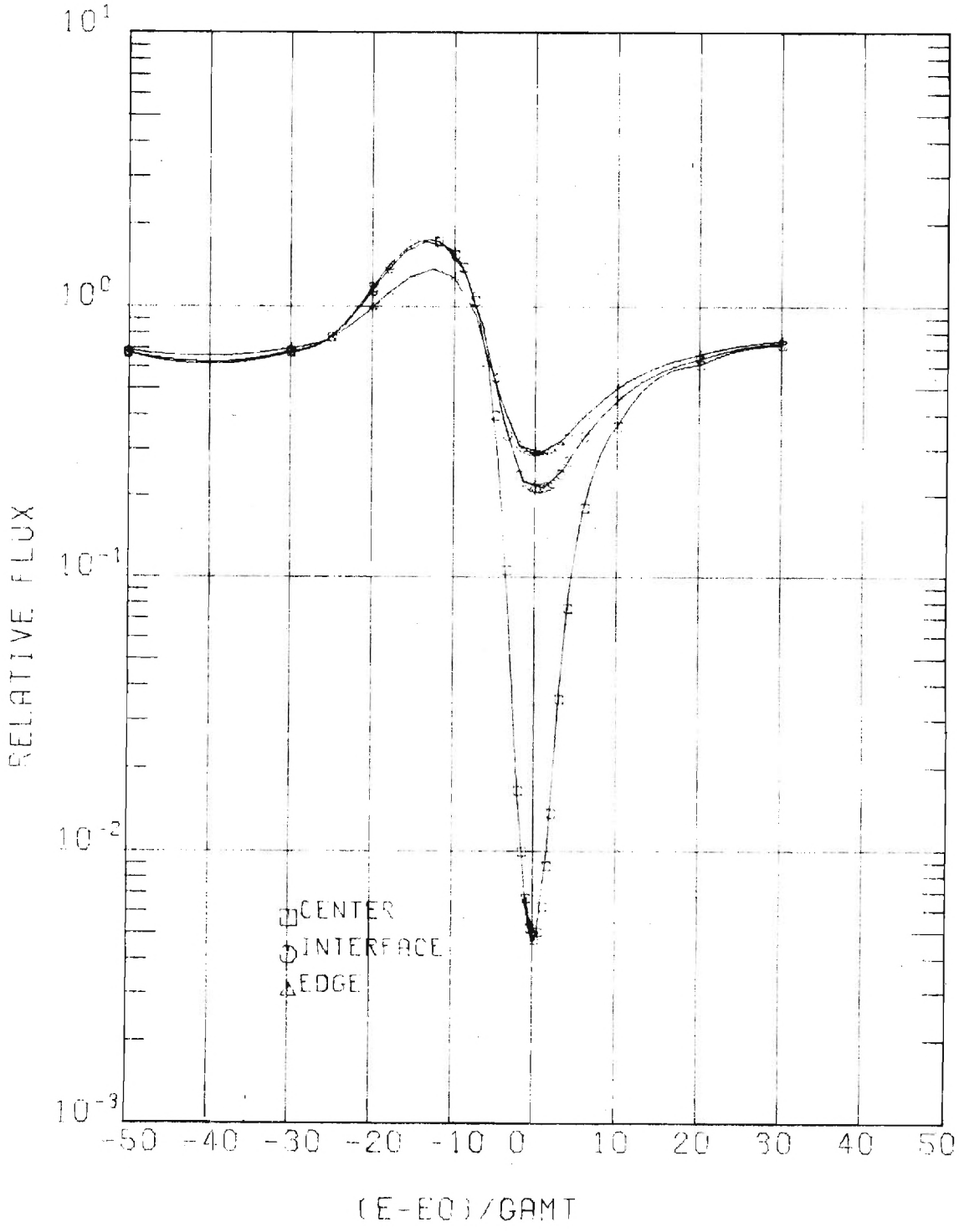

Figure 1. Energy Dependent Flux Around 189.6 eV Resonance

magnitude of the flux depression in the plate and the accompanying depression in the outer region is seen in the example case. The depression of the flux in the plate for the 189.6 eV resonance is seen to be quite large and Fig. 2 shows the spatial flux profile for this resonance at a few energy points. It is such flux depressions that yield nonuniformity in the neutron source as can be seen in Fig. 3. The source nonuniformity is also reflected in the nonuniformity factor f(E) shown in Fig. 4 for each of the three resonances. Recall that f(E) is unity for a flat source, which shows that the slowing-down source through the 1098.1 eV resonance is flat. For the 518.3 eV resonance there is some nonuniformity and a larger amount for the 189.6 eV resonance.

The nonuniformity of the neutron source is also reflected in the shape of the escape cross section as determined by the escape probability for the nonuniform source. Escape cross sections for the three resonances are given in Fig. 5. Comparison to Eq. 51, which is for a flat source, shows no difference for the 1098.1 eV resonance, but differences of over a factor of three near the center of the 189.6 eV resonance. Careful inspection shows, in Fig. 5 and more obviously in Fig. 4, that the effect of nonuniformity is not symmetric about the center of the resonance. For these cases the minimum value of f(E) occurs below the center of the resonance because the slowing-down source below the center has been affected by a larger portion of the resonance than has an equally spaced point above the center. Interference scattering and the accompanying smaller cross section values also affect the shape below the center as the flux and source recover rapidly.

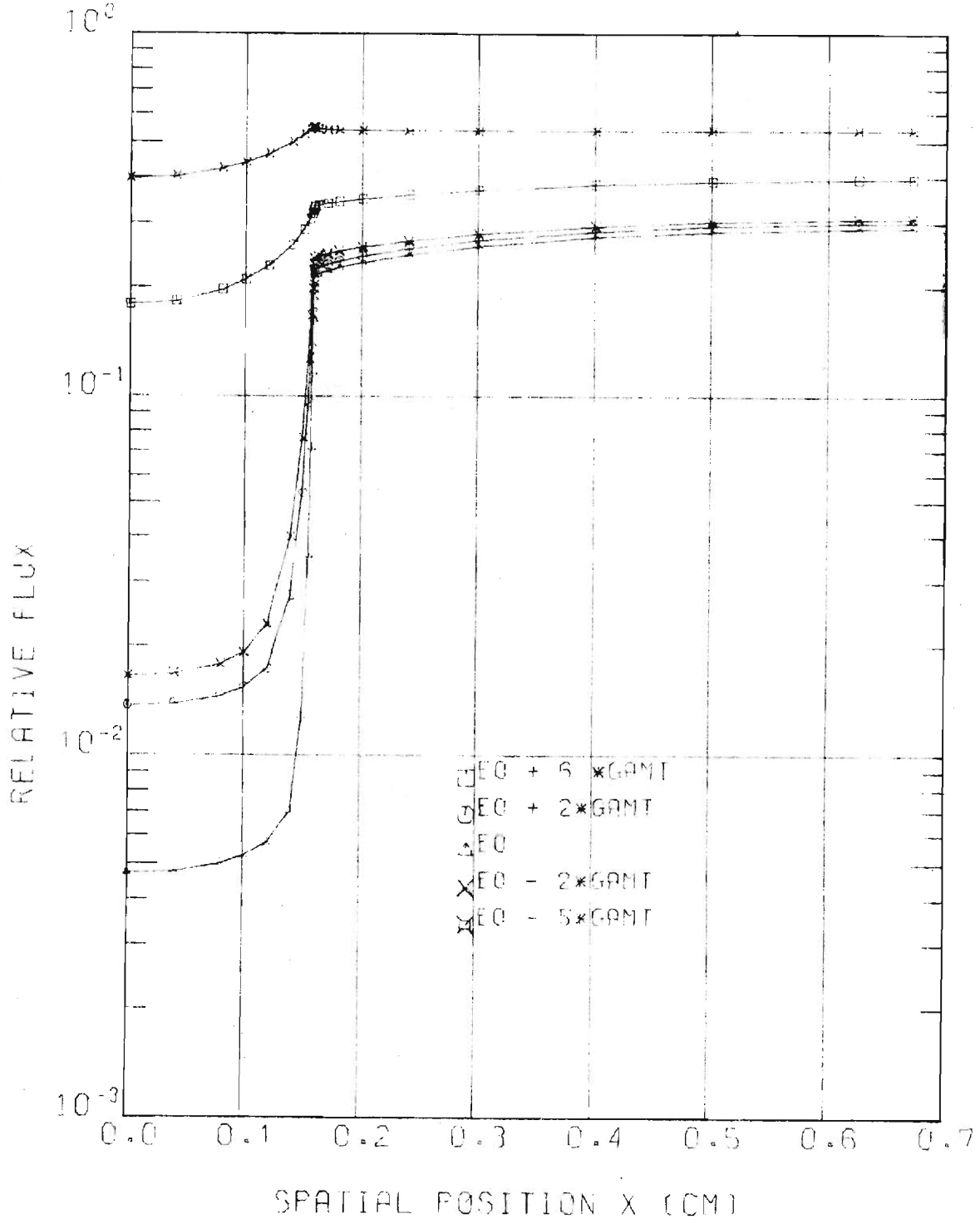

Figure 2. Spatially Dependent Flux for 189.6 eV Resonance

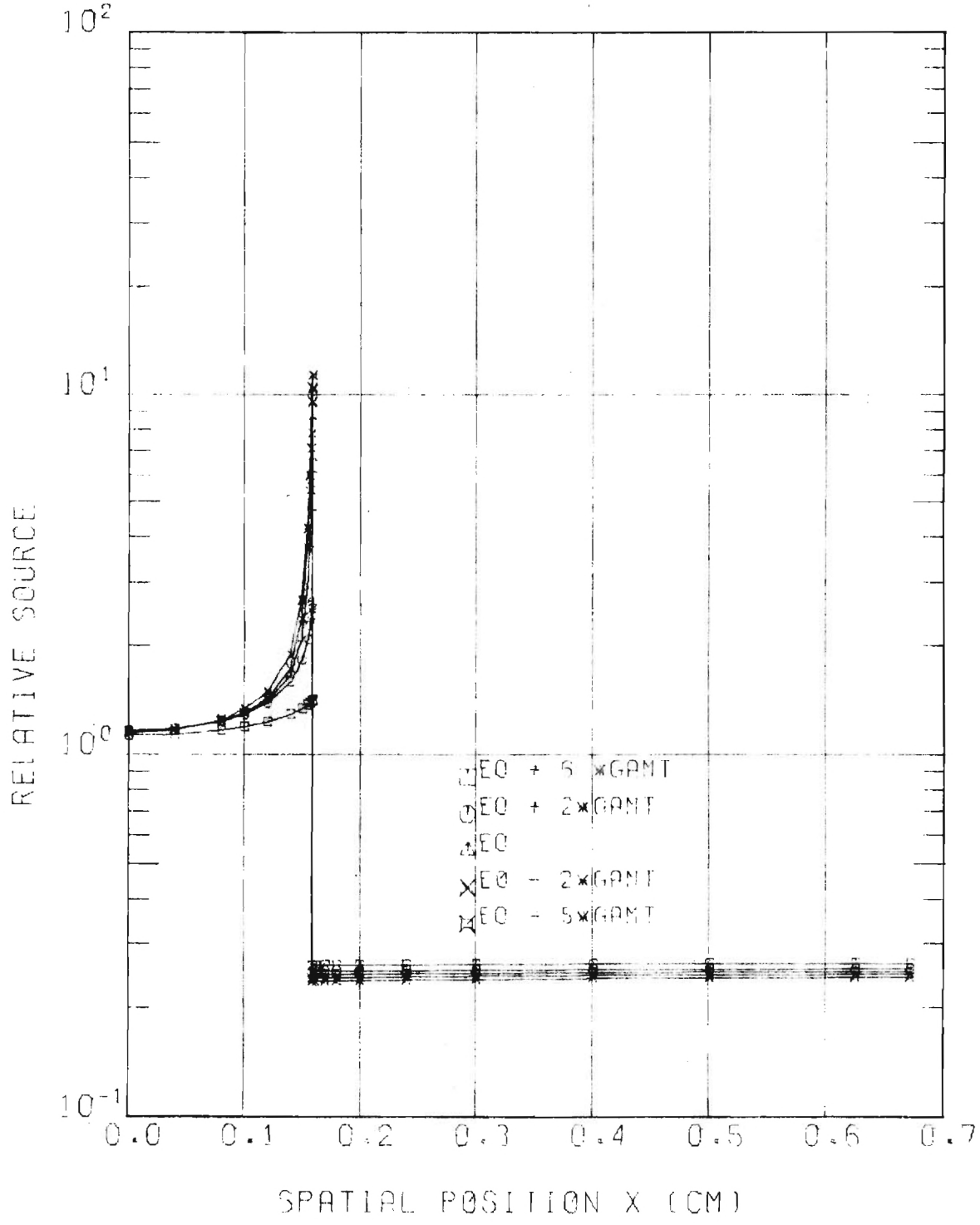

Figure 3. Spatially Dependent Source for 189.6 eV Resonance

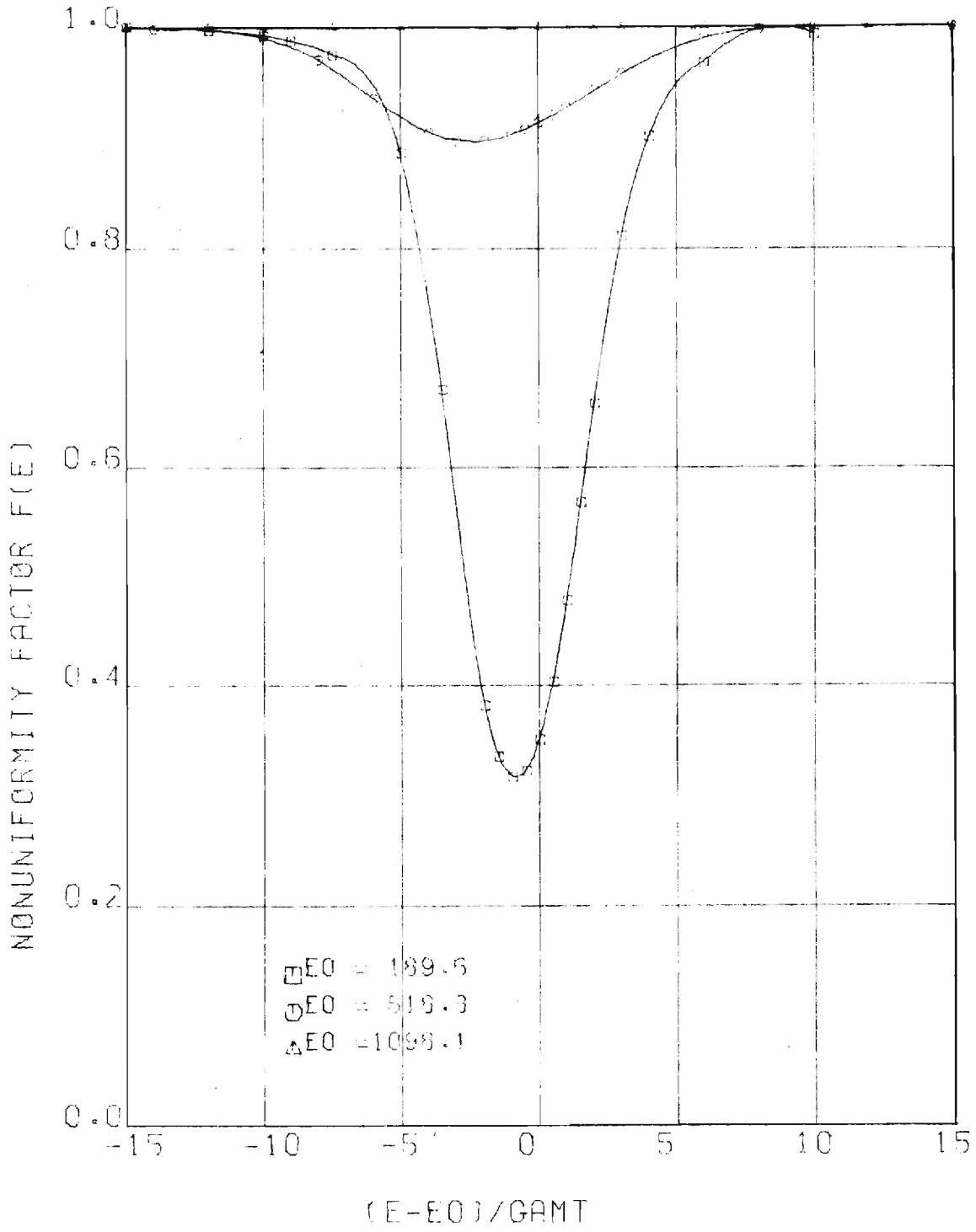

Figure 4. Nonuniformity Factor f(E) for ^{238}U Resonances

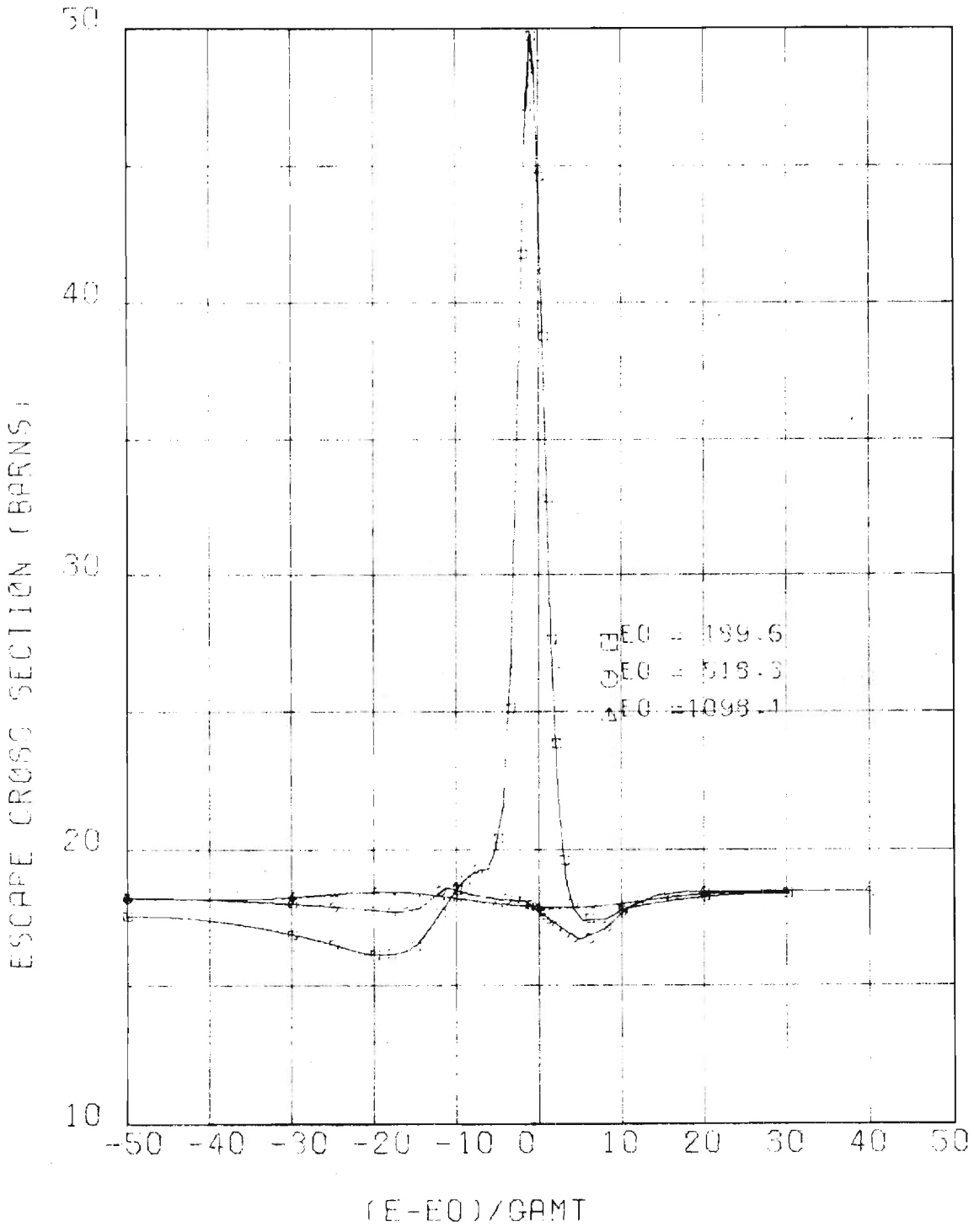

Figure 5. Escape Cross Sections for ^{238}U Resonances

It is instructive to investigate the impact of nonuniformity on the general flux expression given by Eq. 50, using the 189.6 eV resonance of ^{238}U. In this expression the escape cross section appears in the numerator multiplied by f(E) and in the denominator added to the total cross section. Although the escape cross section reflecting the nonuniform source is greater than three times the exact flat value near the center of the resonance, the net difference when comparing the sums with the large total cross section value is only about 1%. The difference between the nonuniform treatment and the exact flat treatment as reflected in the numerator can be seen by comparing $f(E) \times \sigma_e(E)$ for the nonuniform case to the escape cross section for a flat source. For this particular resonance, the product of the factors for the nonuniform case near the center of the resonance is only 3% higher than the escape cross section for a flat source. Hence the effect of nonuniformity of f(E) and $\sigma_e(E)$ combine to compensate, yielding a net result very similar to that for a flat source.

The compensating effect can perhaps be seen more clearly by examination of the escape probability rather than the artificial escape cross section. The reaction rate balance given in the general collision density equation (Eq. 25) and given below for the two-region case,

$$\Sigma_{t_1}(E)\bar{\phi}_1(E) = (1-P_{1\to 2}(E))\bar{\chi}_1(E) + f(E)P_{1\to 2}(E)\frac{\Sigma_{t_1}(E)}{\Sigma_{t_2}(E)}\bar{\chi}_2(E), \qquad (58)$$

provides a mechanism for comparing the difference due to nonuniform or flat-source treatment. For the same source magnitudes with the two treatments, differences in the collision rate expression can be due only to the escape probability and f(E). The specific comparisons to be made are for the term $1-P_{F\to M}(E)$ and for $f(E) \times P_{F\to M}(E)$ for the two treatments.

Such comparisons can be made by examination of Fig. 6 which gives the escape probabilities for the nonuniform source and flat source as well as f(E) times the escape probability for the nonuniform source. The escape probability for the nonuniform source is seen to be significantly greater than that for the flat source near the center of the resonance, but at such points both values are much less than unity. When the nonuniform escape probability is multiplied by f(E) one also sees that compensation results, yielding values very much the same as the exact flat case.

A more detailed assessment of the effects of nonuniformity on the escape probabilities and parameters of the general method, and the potential effects on cross section averaging, require investigation over a larger number of resonances than just the three cases noted above. In order to perform such an assessment then, a parametric evaluation was carried out using artificial resonances which represented the resolved range for ^{238}U. An entire analysis of the 199 resolved s-wave resonances of ^{238}U as given in ENDF/B-III would be prohibitive, but studies of a parametric nature over selected resonance parameters can be used to obtain data for the actual resonances. Four different peak energies and six different neutron widths were considered; a constant capture width of 0.0235 eV was used for each combination. The effects of nonuniformity as reflected by the parameter f(E) were determined by the parametric study. A summary of the effects on this parameter is shown in Fig. 7, which gives the minimum value of f(E) as a function of neutron width for the various peak energies. A comparison of escape probabilities for the nonuniform sources and for a flat source at the peak energy of the resonance is shown in Table III. The compensation effect is also shown in the table by comparison of f(E) times the escape probability of the nonuniform source to

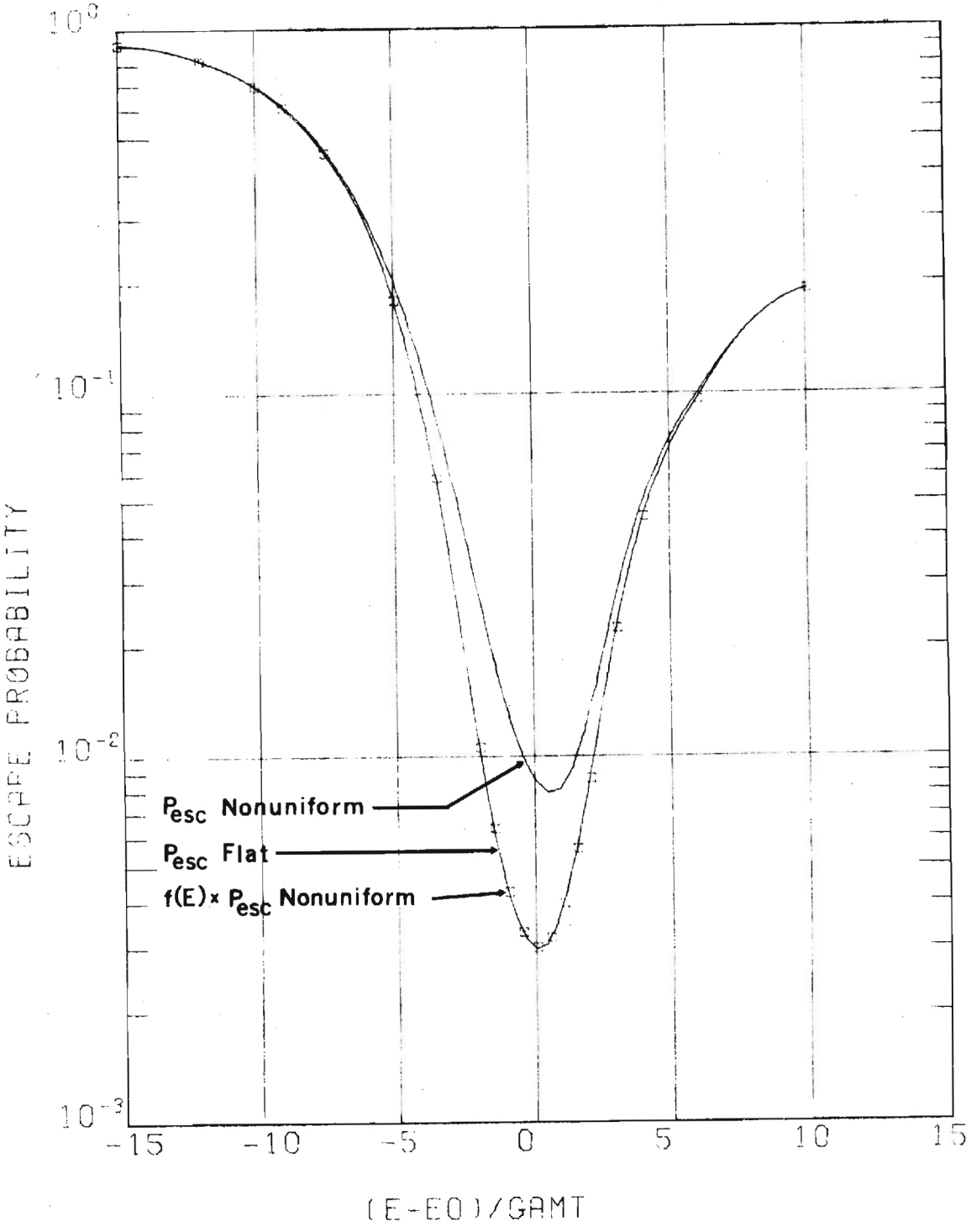

Figure 6. Escape Probability Comparisons for Flat and Nonuniform Sources Around 189.6 eV Resonance

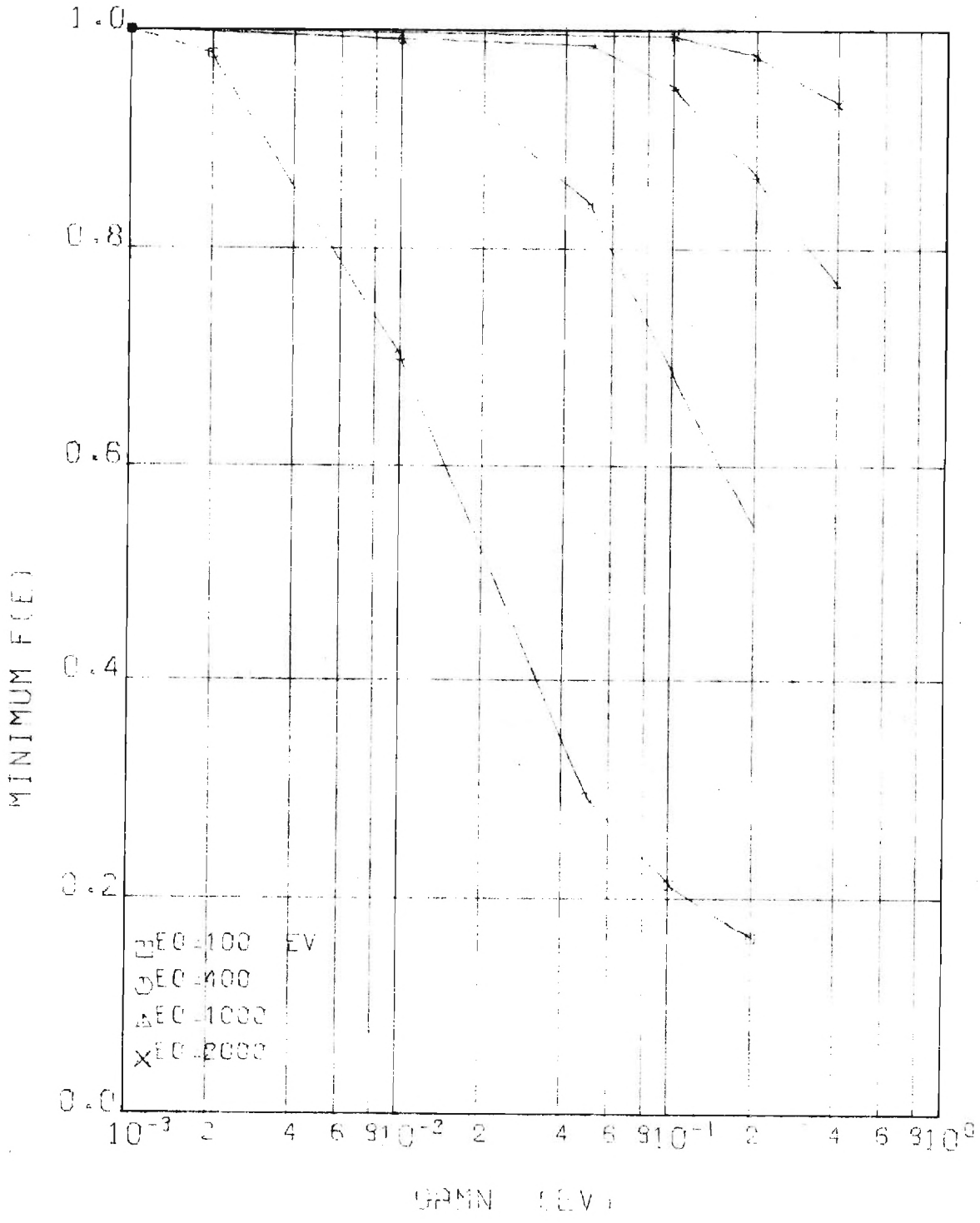

Figure 7. Minimum Values of f(E) as a Function of Neutron Width

Table III. Escape Probability at the Resonance Peak Energy for Parametric Cases

E_o (eV)	Γ_n (eV)	P_{esc} Nonuniform	P_{esc} Flat	$f(E) \times P_{esc}$ Nonuniform
100.	0.002	7.321-2	7.170-2	7.177-2
	0.010	2.068-2	1.527-2	1.534-2
	0.050	1.035-2	3.406-3	3.442-3
	0.100	7.936-3	1.918-3	1.937-3
	0.200	6.490-3	1.186-3	1.193-3
400.	0.010	1.019-1	1.011-1	1.012-1
	0.050	2.713-2	2.293-2	2.293-2
	0.100	1.771-2	1.231-2	1.231-2
	0.200	1.209-2	6.966-3	7.005-3
1000.	0.050	8.157-2	8.048-2	8.054-2
	0.100	4.566-2	4.345-2	4.352-2
	0.200	2.719-2	2.388-2	2.395-2
	0.400	1.789-2	1.395-2	1.402-2
2000.	0.100	1.147-1	1.141-1	1.141-1
	0.200	6.550-2	6.400-2	6.407-2
	0.400	3.906-2	3.653-2	3.661-2

Note: Read values such as 7.321-2 as 7.321×10^{-2}.

the exact flat escape probability.

Additional examination of the parametric cases gave a basis for the compensating effect. It was observed that the probability of neutrons within the outer region escaping into the plate region was never more than 1% different from that for a flat source. This observation can be used to restate the general reciprocity relation of Eq. 48 to the form

$$f(E) = \frac{P_{1\to2}^{flat}(E)}{P_{1\to2}^{Nonuniform}(E)} \tag{59}$$

This expression is possible due to the fact that the numerator of Eq. 48 can be replaced by $P_{1\to2}^{flat}(E)\,\Sigma_{t1}(E)V_1$ according to the flat-flux reciprocity relation of Eq. 22. The escape cross section can then be rewritten as

$$\sigma_e(E) = \frac{\sigma_{t1}(E)P_{1\to2}^{flat}(E)}{f(E) - P_{1\to2}^{flat}(E)}\,. \tag{60}$$

With this simplification the effect of nonuniformity is completely contained in f(E).

In order to extend the data for f(E) from the parametric study to the actual resonances of ^{238}U an interpolation in energy and neutron width was used. The parametric data were first fitted to a consistent mesh because different energy meshes were used in the integral transport calculations, tailored to the particular cross section behavior. A cubic spline interpolation was used to go from the specific meshes to the consistent mesh; from the data in the consistent mesh structure a logarithmic interpolation in energy and neutron width between parametric points was used to obtain f(E) for the actual resonances from the parametric data.

Cross Section Averaging

Having fitted the nonuniformity parameter f(E) to the actual ^{238}U resonances, cross section averages were obtained by the methods noted in Section III. By the same method, averages were calculated using equivalence theory and the exact escape probability treatment for a flat source. For the purpose of cross section averaging the outer region source was assumed to have the asymptotic 1/E shape for all cases. For equivalence theory and the exact flat treatment the plate source was treated by the NR approximation. For the nonuniform source treatment the plate region source was determined by iterative solution of the collision rate expression with the NR approximation as an initial guess.

Cross section averages for the three treatments noted above are given in Table IV for the two-region cell of Assembly 5. Only the resolved s-wave resonances of ^{238}U were included; the energy structure and indices of the broad groups are the same as in Reference 26; the upper bound of group 15 is 4307. eV. From the tabulated results, it can be seen that there is very little difference between the three treatments of heterogeneity. Equivalence theory results are seen to be consistently the smallest, exact flat the largest, with the nonuniform treatment between then; the maximum difference is hardly more than 1% though. The compensating effects which occur in the nonuniform treatment have been noted to tend toward the exact flat treatment, and any remaining effects appear to give slight reductions which tend toward the equivalence theory results.

Table IV. Effective Resonance Cross Sections for the Two-Region Cell of ZPR-6 Assembly 5 (Barns)

Group	E_{lower} (eV)	Equivalence Theory	Exact Flat	Nonuniform
15	2612.	0.3875	0.3925	0.3886
16	2035.	0.5202	0.5275	0.5214
17	1234.	0.5318	0.5425	0.5350
18	961.	0.6443	0.6539	0.6466
19	582.9	0.8005	0.8121	0.8021
20	275.4	0.6871	0.6987	0.6894
21	101.3	1.1224	1.1305	1.1218
22	29.02	1.7327	1.7427	1.7318
23	13.71	2.7702	2.7852	2.7696

In order to obtain independent assessment of the nonuniformity effect on the effective cross sections and to verify the magnitude of the cross sections, comparative calculations were performed. Equivalence theory calculations were performed using the MC^2 module of the Argonne Reactor Computation (ARC) System,[27] and integral transport theory calculations were made with the latest version of the RABBLE code.[23] RABBLE runs were made first with only the two regions of the Assembly 5 cell, then each region was divided into five subregions to determine the effect of nonuniformity.

Before meaningful comparisons could be made between the MC^2 and RABBLE results and the above data, certain differences had to be accounted for. The results of Table IV contain only s-wave resonances so the contribution due to p-wave resonances was removed from the MC^2 results. The RABBLE code was used to determine this contribution by calculating the average capture cross sections with and without the p-wave resonances. The contributions due to unresolved resonances and a background capture

cross section were also removed from the MC^2 data, and the resulting cross section comparison for just the s-wave component is given in Table V.

Table V. Comparative Cross Sections for Two-Region Cell of ZPR-6 Assembly 5 (Barns)

Group	MC^2 Equivalence Theory	RABBLE (2 Regions)	RABBLE (10 Subregions)
15	0.3936	0.4094	0.4072
16	0.6228	0.5619	0.5515
17	0.5489	0.5682	0.5591
18	0.6705	0.7186	0.7092
19	0.8081	0.9056	0.8880
20	0.7242	0.8028	0.7927
21	0.9988	1.3028	1.2899
22	1.2661	1.6410	1.6227
23	2.1474	2.6402	2.6109

There are several areas of difference between the MC^2 and RABBLE data themselves as well as to the results of Table IV; however, taken as a total, there is general agreement among the various calculations. One can also note that the two RABBLE calculations show little change in the cross section when more spatial resolution is included. There is a significant difference in the cross section for group 16 from MC^2 as opposed to the other calculations and this difference is probably due to the large sodium resonance. Sodium was handled by broad group cross sections only in the RABBLE calculations. For the data reflected in Table IV the use of an asymptotic outer region source requires only a total macroscopic cross section, so sodium is not handled separately. The use of a fine-group weighting spectrum within the broad group structure of MC^2 could also yield differences and has a significant effect in the lower energy groups. Comparisons did not show the fine group weighting to be responsible for all differences, but the combination of such differences in treatment as the

fine group weighting, unresolved resonances, background capture, light element treatment, and resonance overlap could easily be responsible for the remaining differences between the results.

Additional tests, using RABBLE, were made for various other types of cells, first with two regions, then with several subregions. The first cell in these additional tests was for ZPR-6 Assembly 6, a plate critical with 1/4 inch U_3O_8 plates. The next cells were hypothetical cells of pin geometry for the core and blanket region of a large LMFBR; a typical cell for a light water reactor (LWR) was also examined. A brief description of the various cells is given in Table VI.

Since the intent of these calculations was to explore the nonuniformity effect on ^{238}U capture cross sections, other materials were handled with broad group cross sections or 1/v cross sections. This treatment may be poor for Na, ^{235}U, and Pu isotopes, but it does afford a consistent basis for comparison. The resulting cross section averages are noted in Table VII. Inspection again shows little difference due to the improved spatial treatment of the source. By two independent methods and for different types of cells, it has then been found that nonuniformity has little effect on average cross sections. Differences of only about 1% can be located. The effects of differences of this magnitude on reactor parameters are judged to be small, and nonuniformity treatment does not appear to be the source of current discrepancies between calculations and experiment.

Table VI. Cell Descriptions for Additional Assessment of Nonuniformity

ZPR-6 Assembly 6	LMFBR Core	LMFBR Blanket	LWR
Plate Region	**Pin Region**	**Pin Region**	**Pin Region**
Thickness: 0.635 cm	Radius: 0.2921 cm	Radius: 0.9525 cm	Radius: 0.479 cm
Composition (10^{24} cm^{-3})	Composition (10^{24} cm^{-3})	Composition (10^{24} cm^{-3})	Composition (10^{24} cm^{-3})
^{238}U 0.0233	^{238}U 0.0184	^{238}U 0.0223	^{238}U 0.0362
^{235}U 0.00017	^{235}U 0.00013	^{235}U 0.00005	^{235}U 0.00106
O 0.0627	O 0.0446	O 0.0396	O 0.0745
	^{239}Pu 0.00285		
Outer Region	^{240}Pu 0.00081	**Outer Region**	**Outer Region**
Thickness: 2.365 cm		Radius: 1.239 cm	Radius: 0.815 cm
Composition (10^{24} cm^{-3})	**Outer Region**	Composition (10^{24} cm^{-3})	Composition (10^{24} cm^{-3})
^{238}U 0.00109	Radius: 0.5236 cm	Na 0.0139	Zr 0.00466
^{235}U 0.00141	Composition (10^{24} cm^{-3})	Fe 0.0212	H 0.0596
Na 0.0116	Na 0.0133	Ni 0.0042	O 0.0298
O 0.00175	Fe 0.0187	Cr 0.0062	
Fe 0.0179	Ni 0.0037		
Ni 0.0017	Cr 0.0049		
Cr 0.0035			

Table VII. ^{238}U Capture Cross Sections for Additional Cell Descriptions (Barns)

Group	ZPR-6 Assembly 6 Cell		LMFBR Core Cell		LMFBR Blanket Cell		LWR Cell	
	2 Regions	10 Subregions	2 Regions	10 Subregions	2 Regions	10 Subregions	2 Regions	10 Subregions
15	0.475	0.473	0.587	0.587	0.453	0.455	0.378	0.378
16	0.670	0.666	0.870	0.874	0.613	0.616	0.486	0.487
17	0.682	0.679	0.936	0.941	0.638	0.642	0.498	0.500
18	0.852	0.849	1.216	1.223	0.792	0.797	0.618	0.620
19	1.101	1.096	1.688	1.701	1.014	1.021	0.756	0.759
20	0.989	0.985	1.579	1.591	0.911	0.917	0.666	0.668
21	1.576	1.568	2.536	2.554	1.461	1.468	1.254	1.257
22	--	--	2.869	2.881	1.843	1.849	--	--
23	--	--	4.685	4.701	2.869	2.880	--	--

V. CONCLUSIONS

From the studies carried out in this work, two primary conclusions are reached. First, through the use of a generalized reciprocity relation and an energy-dependent escape cross section, a method for cross section averaging can be obtained which is simple in form, correctly accounts for flux nonuniformity in space, and includes the more standard approximations as options.[28] Secondly, even though there were significant differences between the exactly calculated escape probabilities and those calculated with the flat-source approximation, additional differences between the general energy-dependent reciprocity relation and the energy-independent (but often erroneously applied as energy-dependent) reciprocity relation almost completely compensated for the error in the flat-source escape probabilities. Due to this unusual and somewhat unexpected compensating effect, the effective capture cross sections of ^{238}U in the resolved resonance region, generated by the three methods stated earlier, were essentially the same (see Table IV).

The neutron source distribution, shown in Fig. 3 for the 189.6 eV resonance, shows that the source in the absorber plate is significantly higher than that in the surrounding medium. The large σ_p of the absorber plate relative to the scattering cross sections of the surrounding medium is the reason why the source is high in the absorber. Under these conditions the resonance integral over the 189.6 eV resonance is largely determined by the source in the plate and not in the surrounding medium.

The magnitude of the neutron source shown in Fig. 3 is largely governed by the value of σ_p and the slowing-down process. The slowing-down

process used was based on the free-gas model (i.e. the absorber atoms are free in a gaseous state) and on the assumption of isotropic elastic scattering in the center of mass coordinates. The free-gas model, as far as we know, has always been used for neutron energies above 1.0 eV. This is certainly the case in such codes as the MC^2, RABBLE, and GAROL.

The source distribution shown in Fig. 3 indicates that in order for σ_c^{238} to be too high in the resonance region, either the value of σ_p for ^{238}U would have to be too high or the resonance parameters would have to be too poorly understood, and highly erroneous, or the slowing-down process would have to unrealistically produce large numbers of resonance neutrons. The potential scattering cross is known to a good accuracy and may be ruled out as a source of major error. The picture with respect to resonance parameters is more complex especially in the unresolved region. However, the magnitude of the differential capture cross section of ^{238}U has been going upward whereas integral measurements required lower values. The slowing-down process based on the free-gas model for crystalline ^{238}U metal may produce large error in the effective, broad group, resonance capture cross sections of ^{238}U.

Consequently, the mechanics of slowing-down in ^{238}U, possibly in the energy loss mechanism or through anisotropic effects, may warrant investigation. In addition to these areas, one must also continue to address the adequacy of the differential cross section data.

REFERENCES

1. G. I. Bell and S. Glasstone, Nuclear Reactor Theory, Van Nostrand Reinhold Co., New York, 1970.

2. L. Dresner, Resonance Absorption in Nuclear Reactors, Pergamon Press, Inc., New York, 1960.

3. G. I. Bell, "Theory of Effective Cross Sections," LA-2322, Los Alamos Scientific Laboratory, October 6, 1959.

4. J. Chernick and R. Vernon, "Some Refinements in the Calculation of Resonance Integrals," Nucl. Sci. Eng., 4, 649 (1958).

5. W. Rothenstein, "Collision Probabilities and Resonance Integrals for Lattices," Nucl. Sci. Eng., 4, 649 (1958).

6. D. C. Leslie, J. C. Hill, and A. Jensson, "Improvements to the Theory of Resonance Escape in Heterogeneous Fuel. 1. Regular Arrays of Fuel Rods," Nucl. Sci. Eng., 22, 78 (1965).

7. G. I. Bell, "A Simple Treatment for Effective Resonance Integrals in Dense Lattices," Nucl. Sci. Eng., 5, 138 (1959).

8. H. H. Hummel, "Equivalence Between Homogeneous and Heterogeneous Resonance Integrals in Cylindrical Geometry," Reactor Physics Div. Annual Report, July 1, 1964 to June 30, 1965, ANL-7110, Argonne National Laboratory, 319 (1966).

9. M. M. Levine, "Resonance Integral Calculations for U^{238} Lattices," Nucl. Sci. Eng., 16, 271 (1963).

10. C. N. Kelber, "Improved Rational Escape Probability in Lumped Absorbers," Nucl. Sci. Eng., 22, 224 (1965).

11. Charles N. Kelber, "An Extended Equivalence Relation," Nucl. Sci. Eng., 42, 257 (1970).

12. A. Travelli, "A Modification of the Bell Approximation for Slab Geometries," Reactor Physics Division Annual Report, July 1, 1967 to June 30, 1968, ANL-7410, Argonne National Laboratory, 424 (1969).

13. L. W. Nordheim, "A New Calculation of Resonance Integrals," Nucl. Sci. Eng., 12, 457 (1962).

14. L. W. Nordheim, "A Program of Research and Calculations of Resonance Absorptions," GA-2527, General Atomic, August 28, 1961.

15. E. E. Lewis, "A Boltzmann Integral Equation Treatment of Resonance Absorption in Reactor Lattices," Ph.D. Thesis, University of Illinois, 1965.

16. E. E. Lewis and F. T. Adler, "A Boltzmann Integral Equation Treatment of Neutron Resonance Absorption in Reactor Lattices," Nucl. Sci. Eng., 31, 117 (1968).

17. P. H. Kier, "RIFF RAFF, A Program for Computation of Resonance Integrals in a Two-Region Cell," ANL-7033, Argonne National Laboratory, August 1965.

18. A. P. Olson, "RABID: Integral Transport Theory Code for Neutron Slowing Down in Slab Cells," ANL-7645, Argonne National Laboratory, 1970.

19. D. C. Irving, "The Adjoint Boltzmann Equation and Its Simulation by Monte Carlo, "ORNL-TM-2879, Oak Ridge National Laboratory, May 18, 1970.

20. E. P. Wigner, E. Creutz, H. Jupnik, and T. Snyder, "Resonance Absorption of Neutrons by Spheres," J. Appl. Phys., 26, 260 (1955).

21. C. A. Stevens and C. V. Smith, "GAROL, A Computer Program for Evaluating Resonance Absorption Including Resonance Overlap," GA-6637, General Atomic, August 24, 1965.

22. Hellen M. Summer, "ERIC-2, A Fortran Program to Calculate Resonance Integrals and From These Effective Capture and Fission Cross Sections," AEEW-R 323, Atomic Energy Establishment, Winfrith, 1964.

23. P. H. Kier and A. A. Robba, "RABBLE, A Program for Computation of Resonance Absorption in Multiregion Reactor Cells," ANL-7326, Argonne National Laboratory, April 1967.

24. Anthony Ralston and Herbert S. Wilf, Ed., Mathematical Methods for Digital Computers, Volume II, John Wiley & Sons, Inc., New York, 1967, p. 133.

25. K. M. Case, F. de Hoffman, and G. Placzek, Introduction to the Theory of Neutron Diffusion, U. S. Gov't. Printing Office, Washington, D. C., 1953.

26. R. A. Karam, J. E. Marshall, and K. D. Dance, "Analysis of Heterogeneity and Sodium-Void Effects in a 2700-Liter Uranium Carbide Fast Core, ZPR-6 Assembly 5," Nucl. Sci. Eng., 43, 5 (1971).

27. L. C. Just, H. Henryson, II, A. S. Kennedy, S. D. Sparck, B. J. Toppel, and P. M. Walker, "The System Aspects and Interface Data Sets of the Argonne Reactor Computation (ARC) Series," ANL-7711, Argonne National Laboratory, 1971.